Alma Mater Studiorum Università di Bologna
Archivio istituzionale della ricerca

Inhibition of Urease, a Ni-Enzyme: The Reactivity of a Key Thiol With Mono- and Di-Substituted Catechols Elucidated by Kinetic, Structural, and Theoretical Studies

(Article begins on next page)

04 May 2024

Inhibition of urease, a Ni-enzyme: the reactivity of a key thiol with mono- and di-substituted catechols elucidated by kinetic, structural and theoretical studies

Luca Mazzei,[a,c,*] Umberto Contaldo,[a,b] Francesco Musiani,[a,c] Michele Cianci,[d] Greta Bagnolini,[a] Marinella Roberti,[a] Stefano Ciurli [a,c,*]

[a] Department of Pharmacy and Biotechnology (FaBiT), University of Bologna, Via Belmeloro 6, I-40127 Bologna (Italy)

[b] Laboratory of Chemistry and Biology of Metals, Université Grenoble Alpes, CEA, CNRS, 17 Avenue des Martyrs, F-38000 Grenoble, France

[c] Laboratory of Bioinorganic Chemistry, Department of Pharmacy and Biotechnology (FaBiT), University of Bologna, Via Giuseppe Fanin 40, I-40127 Bologna (Italy)

[d] Department of Agricultural, Food and Environmental Sciences, Polytechnic University of Marche Ancona (Italy)

* Corresponding authors: stefano.ciurli@unibo.it; luca.mazzei2@unibo.it

ABSTRACT

Urease is a Ni(II)-containing enzyme able to catalyse the conversion of urea to ammonia and carbamate. Urea, the most used soil nitrogen fertiliser worldwide, is thus rapidly hydrolysed into species of nitrogen that can be taken up by plants, a function that, while essential, might also significantly decrease the efficiency of this process due to the release of gaseous species of nitrogen into the atmosphere, contributing to the green-house effect and to air pollution. Moreover, urease is also a virulence factor for ureolytic bacterial human pathogens that affect the health and livelihood of millions of people, especially, but not only, in developing nations of Africa, Asia and Latin America. For these reasons, strategies for the efficient inhibition of urease activity by molecules that interact with the enzyme and counterbalance its negative effects must be pursued. Here, the inhibition of urease from *Sporosarcina pasteurii* (SPU) and *Canavalia ensiformis* (jack bean, JBU) by a class of six aromatic poly-hydroxylated molecules, namely mono- and dimethyl-substituted catechols, was investigated on the basis of the inhibitory efficiency of the catechol scaffold. The aim was to probe the key step of a mechanism proposed for the inhibition of SPU by catechol, namely the sulfanyl radical attack on the aromatic ring, as well as to obtain critical information on the effect of substituents of the catechol aromatic ring on the inhibition efficacy of its derivatives. The crystal structures of all six SPU-inhibitors complexes, determined at high resolution, as well as kinetic data obtained on JBU and theoretical studies of the reaction mechanism using quantum mechanical calculations, revealed the occurrence of an irreversible inactivation of urease by means of a radical-based autocatalytic multistep mechanism, and indicate that, among all tested catechols, the mono-substituted 3-methyl-catechol is the most efficient inhibitor for urease.

INTRODUCTION

Urease is a non-redox nickel-enzyme found in plants, algae, fungi, and several microorganisms [1], operating in the global nitrogen cycle while catalysing the rapid hydrolytic decomposition of urea to give ammonia and carbamate [2]. This reaction causes an overall increase of pH that has negative consequences for both human health [3] and the environmental ecosphere [4]. In particular, urease is exploited as a virulence factor by several human pathogens [3, 5] including *Helicobacter pylori* [6], *Staphylococcus aureus* [7], *Mycobacterium tuberculosis* [8], *Yersinia enterocolitica* [9] and *Cryptococcus neoformans* [10], thus acting as a threat to public health worldwide. Moreover, the priority pathogen list indicated by the World Health Organization for the research and development of new antibiotics includes several urease-dependent antibiotic-resistant bacteria, many of which are involved in bacterial infections of the respiratory apparatus [11]. It is remarkable that half of patients who died of the recent COVID-19 epidemics in Wuhan (China) became co-infected with bacteria in the lungs and also required antibiotics [12]. Furthermore, the widespread presence of urease in soils causes the release of large amounts of nitrogen, in the form of ammonia, in the atmosphere, thus decreasing the efficiency of urea-based soil fertilization with the consequent formation of airborne particulate matter (PM) that contributes to atmospheric pollution [13]. It has been found that the presence of ultrafine PM has been significantly associated with an increase of the mortality rate in the SARS (Severe Acute Respiratory Syndrome) epidemics in the early 2000's [14], suggesting that containment of air pollution through well-managed agricultural activities is absolutely necessary not only for the environment, but also for human health.

The active site of urease comprises a fully conserved bimetallic Ni(II) cluster located in a pocket covered by a conserved 30-residues helix-turn-helix motif, also called "mobile flap" (Figure 1). The mobile flap carries, at the tip of its turn region, a largely conserved Cys residue and a fully conserved His residue (αCys322 and αHis323 according to *Sporosarcina pasteurii* (*Sp*) urease (SPU) numbering) [15]. Integrated crystallographic and kinetic studies performed on SPU in the native state [16] and inhibited by several compounds [2d, 15-17], as well as in complex with the substrate urea [18],

established that the mobility of the flap, able to adopt an open and a closed conformation by a positional *ca*. 5-Å shifting of the αCys322 and αHis323 residues with respect to the active site di-nickel cluster, is a crucial feature exploited by urease to efficiently regulate its catalytic mechanism during the main enzymatic reaction steps. In particular, the open state of the flap allows substrate access into, as well as products release from, the active site cavity, while the closed state causes the reduction of volume of the active site cavity, with the flap stabilizing both the substrate urea bound in a chelating mode to the di-nickel cluster and the tetrahedral diamino-methane-diol intermediate that forms following the nucleophilic attack on the urea carbonyl C atom [17b, 17h, 17k, 17l, 18-19].

In general, the urease inhibitors characterized so far belong to two main categories, based on their mode of interaction with the enzyme. The first group encompasses compounds that directly bind to the Ni(II) ions in the active site (such as phosphorodiamidate [17b] and its modified forms [17h], phosphate [17d], thiols [17a], sulfite [17f], fluoride [16], as well as hydroxamic [17c], citric [20] and boric [17e] acids), while the second group comprises compounds proven to bind to the Sγ atom of the mobile flap conserved Cys residue (such as 2-mercapto-ethanol (BME) [17a], 1,4-benzoquinone (PBQ) [17g], catechol (CAT) [17i] and heavy transition metal ions such as silver(I) [15] and gold(I) [17j]). In particular, the structures of SPU inactivated by CAT and PBQ show that the thiol group of αCys322 forms a covalent adduct with the ligands, blocking enzyme activity by rendering the flap unable to switch from an open to a closed state. Similarly, SPU inhibited by Ag(I) and Au(I) shows how a di-metallic cluster of these soft acids and heavy transition metal ions blocks the movement of the flap by coordinating the conserved triad composed by αCys322, αHis323 and αMet367 [15, 17j].

Among the cited inhibitors, catechol (CAT) is one of the most effective in inhibiting urease activity [17i]. Kinetic studies performed on urease inactivation by CAT were effectively interpreted using a mathematical model based on a mechanism for the formation of the catechol-enzyme adduct that involves the irreversible inactivation of urease via a complex radical-based autocatalytic multistep reaction [17i]. In particular, this mechanism (Scheme 1) entails an initial oxidation step of CAT by dissolved molecular oxygen to yield the corresponding *ortho* semiquinone (OSQ) as well as the *ortho*

benzoquinone (OBQ) (steps 1 and 2). The comproportionation of OBQ and CAT would yield additional OSQ in an autocatalytic process (step 3). The OSQ subsequently extracts the thiol hydrogen atom of αCys322 to regenerate catechol and yield the sulfanyl radical of the same residue (step 4). The latter then carries out a radical attack on the aromatic carbon atom adjacent to one of the two hydroxyl groups on catechol, producing a radical reaction intermediate featuring a covalent bond between the αCys322 sulphur atom and the aromatic ring of catechol (step 5). The latter radical can be eventually stabilized by a third molecule able to extract a radical H atom and give the reaction product observed in the crystal structure of catechol-bound SPU (step 6). This third player could be either molecular oxygen or superoxide, or another molecule of OSQ (to give the fully reduced catechol), or OBQ (to give OSQ).
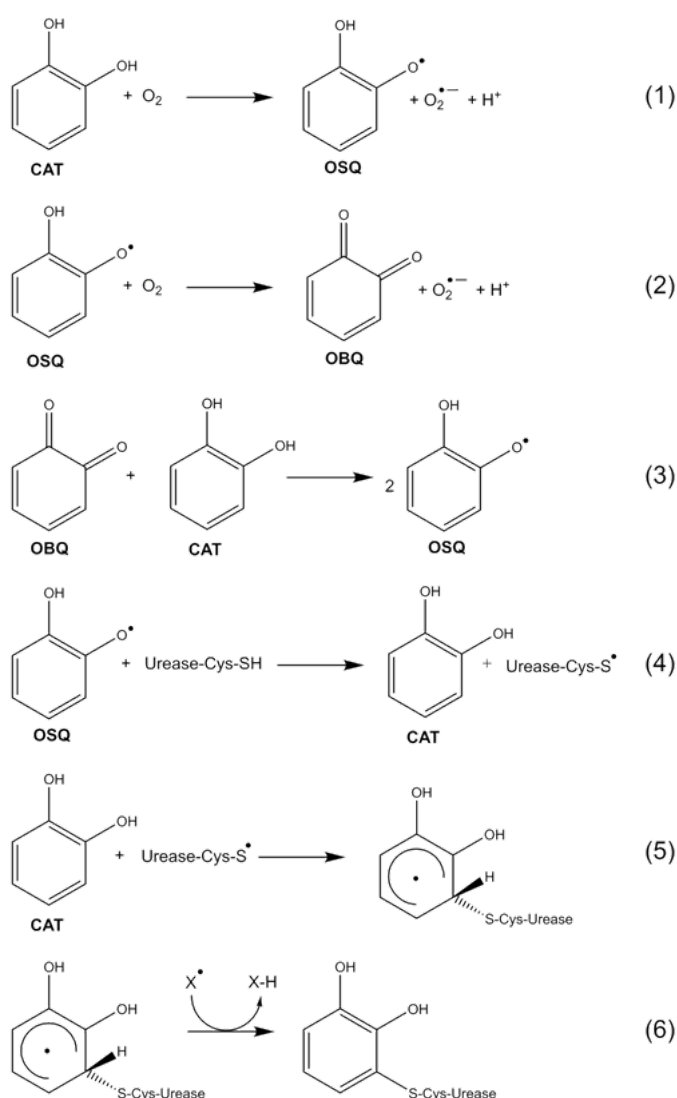
Scheme 1. Working hypothesis for the mechanism of inactivation of urease by catechol.

The present study, aimed at probing the key step of this mechanism, namely the sulfanyl radical attack on the aromatic ring (step 5 in Scheme 1), was carried out using a series of six mono- and di-substituted methyl-catechols (depicted in Scheme 2) through an experimental approach involving kinetic enzymatic assays and X-ray crystallography, with the observations rationalized by quantum-mechanical calculations. The results, described and discussed here below, provide critical information for the inhibition mechanism of urease by means of polyphenols, molecules that comprise a wide class of natural compounds found in fruits, vegetables, cereals, tea, coffee and wine, generally recognized as beneficial to human health for their antioxidant properties [21]. This class of urease inhibitors has also been recently described as efficient against *H. pylori*, but their mode of action has not been understood so far [22].
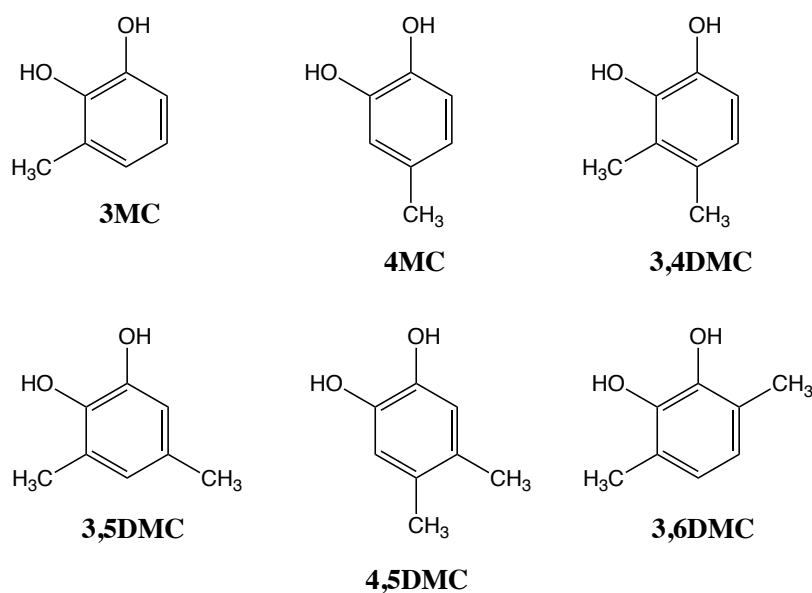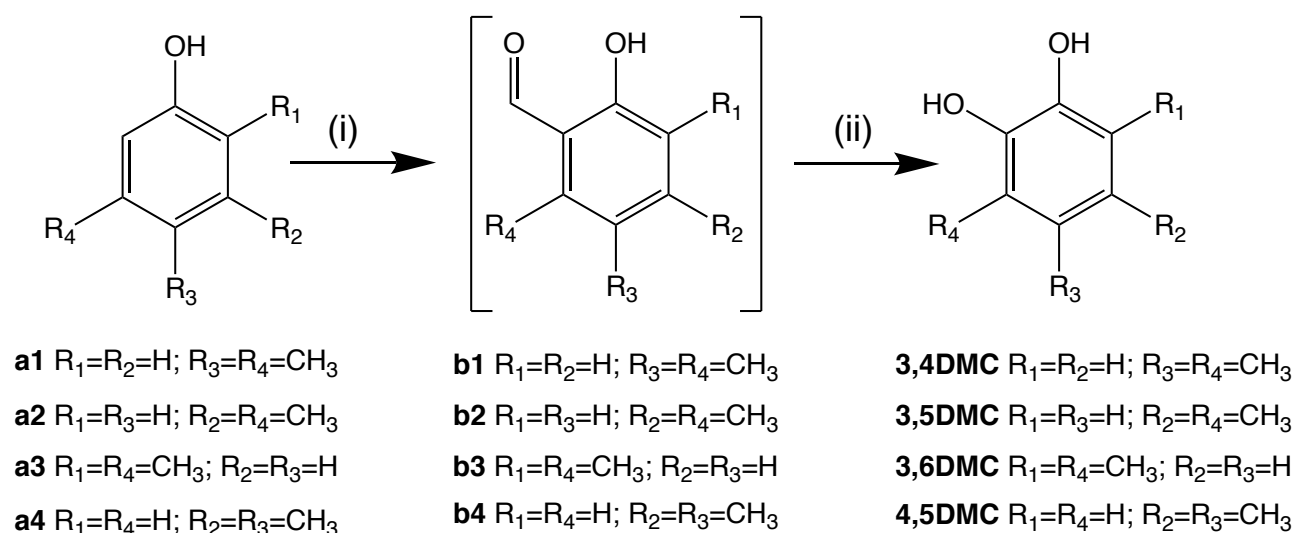

Scheme 2. Structures of the mono- and di-substituted catechol derivatives investigated as urease inhibitors in the present study.

MATERIALS AND METHODS

Sources of catechol derivatives

The mono-substituted catechol derivatives **3MC** and **4MC** were purchased from Sigma-Aldrich (St. Louis, MO). The di-substituted catechols **3,4DMC, 3,5DMC, 4,5DMC 3,6DMC** were

synthetized as shown in Scheme 3. The general synthesis [23] of dimethylbenzene-1,2-diols [24] started from the appropriate dimethylphenol (**a**), which underwent ortho-selective formylation in the presence of $MgCl_2$, TEA and *p*-formaldehyde to achieve the intermediate aldehydes (**b**). Subsequent oxidation by the Dakin reaction in the presence of NaOH and H_2O_2 provided the final compounds.

a1 $R_1=R_2=H$; $R_3=R_4=CH_3$
a2 $R_1=R_3=H$; $R_2=R_4=CH_3$
a3 $R_1=R_4=CH_3$; $R_2=R_3=H$
a4 $R_1=R_4=H$; $R_2=R_3=CH_3$

b1 $R_1=R_2=H$; $R_3=R_4=CH_3$
b2 $R_1=R_3=H$; $R_2=R_4=CH_3$
b3 $R_1=R_4=CH_3$; $R_2=R_3=H$
b4 $R_1=R_4=H$; $R_2=R_3=CH_3$

3,4DMC $R_1=R_2=H$; $R_3=R_4=CH_3$
3,5DMC $R_1=R_3=H$; $R_2=R_4=CH_3$
3,6DMC $R_1=R_4=CH_3$; $R_2=R_3=H$
4,5DMC $R_1=R_4=H$; $R_2=R_3=CH_3$

Scheme 3. General synthesis for dimethyl-substituted catechols. Reagents and conditions: (i) $MgCl_2$ anhydrous, Et_3N, MeCN, *p*-formaldehyde, 100 °C, 2.5 h; (ii) NaOH 5 M, H_2O_2 30%, THF, H_2O, 0 – 25 °C.

The general procedures and characterizations of each dimethyl-substituted catechol **3,4DMC**, **3,5DMC**, **4,5DMC** and **3,6DMC** are reported in the Supplementary Information.

Enzymes sources

Sporosarcina pasteurii urease (SPU), used in this work for crystallographic studies, was expressed and purified from the native source, following a previously reported protocol [17a, 17f, 17g] and stored at +4 °C. *Canavalia ensiformis* (jack bean) urease (JBU) type C-3, powder (≥ 600,000 units/g), used for the kinetic characterization of enzyme inhibition, was purchased from Sigma-Aldrich (St. Louis, MO), dissolved in 20 mM HEPES buffer at pH 7.5, quantified following the manufacturer's information and stored as stock aliquots at -80 °C.

Kinetic measurements

Pre-incubation experiments were carried out at room temperature by using a spectrophotometric assay in which cresol red is exploited as a colorimetric probe to follow the overtime increase of pH due to urease activity, following a protocol previously described [16g]. A reaction mixture was prepared by diluting a 100 nM active JBU stock solution to 1 nM final concentration in a cresol red reaction buffer, the latter containing 30 mg L^{-1} cresol red dissolved in 2 mM HEPES buffer at pH 7.5, also containing 2 mM EDTA. Each inhibitor, in turn dissolved in the same buffer, was added to the reaction mixture to a final 20 μM concentration, taking the time when the enzyme and the inhibitor were mixed as zero time of incubation. After appropriate periods of time, aliquots were withdrawn from the incubation solution, 100 mM urea was added and the change in absorbance over time was monitored (λ = 573 nm). The activity was calculated by a linear fitting of the straight portion in the absorbance *vs*. time curve and normalized to the activity measured at time zero incubation. The residual activity *vs*. time data were fitted using the following Equation 1:

$$[\text{JBU}_{\text{act}}] = [\text{JBU}_{\text{act}}]_0 exp(-k_1 t - k_2 t^2) \qquad \text{(Eq. 1)}$$

This equation was originally derived [16i] assuming the autocatalytic radical-based mechanism described in Scheme 1. In this equation, the values of k_1 and k_2 are used in the present context as kinetic parameters to compare the efficiency of the different substituted catechols in urease inhibition.

Crystallization, data collection and structural determination

The full details of the crystallisation steps are provided in the Supplementary Information. Diffraction data were collected at 100 K using synchrotron X-ray radiation. Datasets of SPU crystals grown in the presence of compounds **3MC**, **4MC** and **3,5DMC** were recorded at the EMBL P13 beamline of the Petra III storage ring, c/o DESY, Hamburg (Germany) [27]. Datasets of SPU crystals grown in the presence of compounds **4,5DMC** and **3,6DMC** were recorded at ID30-A beamline of the ESRF storage ring, Grenoble (France) [28], while the dataset of SPU crystal grown in the presence

of compound **3,4DMC** was recorded at XRD-2 beamline of ELETTRA Synchrotron, Trieste (Italy) [29]. When the crystal dimensions were suitable, helical scanning was performed during data collection to achieve higher data quality by minimizing radiation damage.

Data processing and reduction was carried out using XDS [30] and AIMLESS [31]. The crystals, isomorphous with all the crystal structures of SPU determined so far, belonged to space group $P6_322$. Initial phases for the structure determination were estimated using the structure of SPU inhibited in the presence of catechol (PDB code 5G4H, 1.50 Å resolution) [16i] as a phasing model, devoid of solvent molecules and ligands, and after coordinates randomization in order to remove any potential phase bias. Rigid body and restrained refinement procedures were carried out using REFMAC5 [32]. Model rebuilding, as well as water or ligand addition/inspection were manually conducted using COOT [33]. Unbiased omit maps for non-proteinaceous ligands were calculated with Fourier coefficients F_o - F_c and phases from the last cycle of refinement before addition of the ligand in the models. The models were checked with the PDB REDO web server [34] and deposited in the Protein Data Bank with the accession codes 6ZNY for **3MC**, 6ZNZ for **4MC**, 6ZO0 for **3,4DMC**, 6ZO1 for **3,5DMC**, 6ZO2 for **4,5DMC** and 6ZO3 for **3,6DMC**. The modified Cys-ligand adducts were renamed in the PDB files as follows: QNW for Cys-**3MC**, QNQ for Cys-**4MC**, QO8 for Cys-**3,4DMCT**, QO5 for Cys-**3,5DMC**, QO2 for Cys-**4,5DMC**, QNT for Cys-**3,6DMC**. Data collection and final refinement statistics are given in Table 1-SI. Figures were generated using PyMol (The PyMOL Molecular Graphics System, v. 1.8 Schrödinger, LLC.), and CrystalMaker v. 10.5.4 (http://www.crystalmaker.com).

Quantum mechanical calculations.

Density functional theory (DFT) computations were carried out using the program ORCA 4.1.0 [25] and the Becke three-parameter hybrid functional combined with Lee-Yang-Parr correlation functional [26] as defined in the Gaussian software [27] (B3LYP/G). The full details are provided in the Supplementary Information.

RESULTS AND DISCUSSION

The inhibition kinetics of urease by the mono- and di-substituted catechol derivatives shown in Scheme 2 was investigated using pre-incubation experiments. Our prior knowledge on the negative impact that sodium sulfite (Na_2SO_3), a preservative needed to maintain SPU in an active form [17f], had on urease inactivation by catechol [17i] led us to the use of JBU, the latter not requiring sulfite, as a model enzyme to detect the inhibition properties of the six compounds. The enzyme was incubated with a fixed 20 μM concentration of each inhibitor for increasing periods of time in the absence of substrate, and the residual activity was monitored using a spectrophotometric assay [17g]. The obtained results, presented in Figure 2, show, in all cases, a time-dependent behaviour of enzyme inhibition, with an initial lag phase that evolves into a faster inactivation process eventually yielding the complete abolishment of enzyme activity. This performance is analogous to that previously observed for the inhibition of JBU by CAT [17i], suggesting the occurrence of an analogous inhibition mechanism involving a radical-based autocatalytic multistep process (Scheme 1). That mechanism, for catechol, yields the formation of a covalent bond between the aromatic C atom of the ligand in the *ortho* position to one of the two hydroxyl groups and the thiol functionality of the conserved αCys322 located on the mobile flap that modulates the opening and closing of the active site channel [17i]. As a consequence, the mobility of the flap, essential for catalysis as recently proven [15, 17g-j, 17l, 18] is blocked, with the flap rigidly held in the open conformation, impeding the enzymatic activity.

In order to understand the structural basis of urease inactivation by mono- and di-substituted catechols, and to probe the generality of the mechanism depicted in Scheme 1, a crystallographic study was carried out. SPU was incubated with the six catechol-derivatives shown in Scheme 2 for a proper period of time in order to allow complete inactivation of the enzyme prior crystallization. The obtained crystals were amenable to X-ray diffraction analysis, yielding high-resolution structures (see Table 1-SI for the full details of X-ray data collection, processing and analysis). The resulting SPU crystal structures show a three-dimensional scaffold consisting of the typical (αβγ)₃ trimer of trimers quaternary structure observed in *Sporosarcina pasteurii* and most of the other bacterial ureases. The

structures are mainly coincident with those of the native enzyme (PDB code 4CEU) and catechol-bound SPU (PDB code 5G4H), as depicted by the low values of Cα RMSD calculated on subunits α, β, and γ (Table 2-SI). This overall structural conservation is also confirmed by the analysis of the *per* residue Cα RMSD of subunits α, β, and γ, compared to those of the native and catechol-bound structures (Figures 1-SI and 2-SI). The structural evaluation also highlights a full conservation of the architecture and the coordination environment of Ni(II) ions in active site (Table 3-SI and Figure 3). Concerning the mobile flap region (residues 310-340 of subunit α), a more detailed analysis of the Cα RMSD points out the adoption of an open conformation for all the determined structures, with values lower than 1 Å with respect to the native enzyme, the latter also presenting an open flap (Figure 1-SI). A parallel comparison conducted on the structures under study with respect to the catechol-bound SPU shows even lower Cα RMSD values, suggesting a very consistent positioning of the amino acid residues belonging to that region (Figure 2-SI). Additional electron densities were detected in the vicinity of the αCys322 residue by analysing the F_o - F_c omit maps (Figure 3-SI). These densities were successfully modelled as **3MC**, **4MC**, **3,4DMC**, **3,5DMC**, **4,5DMC** and **3,6DMC**, respectively. All the refined structures feature a covalent bond between αCys322 Sγ atom and an aromatic C atom of each inhibitor, with a constant C-S distance of 1.7 Å (Figures 3 and 4, Table 4-SI). In addition, the two hydroxyl groups of the aromatic compounds point towards the Ni(II) ions, as previously described for catechol [17i], with the peculiar exception of the structure of SPU bound to **3,6DMC**, in which its chemical structure imposes the two OH groups to point toward the protonated amine group of the αLys169 side chain. The overall structural comparison of all the structures determined in the present work, together with the structure of SPU bound to unsubstituted catechol revealed that, in all the cases, the aromatic moiety is largely superimposable (Figure 4-SI). As already observed for the structure of catechol-bound urease, neither αCys520 nor αCys555, two additional solvent-exposed cysteines, bind any catechol derivative, emphasizing the peculiarity of αCys322 residue in the participation of this kind of binding.

The hydrogen-bond network established between the ligand moieties and the surrounding water molecules has been analysed to provide information on the position of hydrogen atoms of the modified residues (Figure 5-SI refers to the case of **3MC** as a representative example). A first well-ordered and conserved water molecule (W_A) acts as H-bonding donor to the backbone carbonyl O atoms of αLys169 and αLeu365 while receiving an H-bond from the protonated O2 atom of the catechol derivatives (O1 atom according to **3,6DMC** numbering). A second well-ordered water molecule (W_B) acts as H-bonding donor to the carbonyl O atoms of αLys169 and αAla366 while receiving an H-bond from the protonated O1 atom of the catechol derivatives; W_B is observed slightly shifted in the structure of urease bound to **3,4DMC**, whereas is not observed in the structure of urease bound to **3,6DMC**, because of the lack of one of the two hydroxyl groups in that position, the latter being replaced by a methyl group. Additionally, another water molecule (W_c) is sometimes observed within the active site cavity, H-bonded to W_B and to the distal water molecule belonging to the tetrahedral solvent cluster in the vicinity of the Ni(II) ions.

A comparison of the X-ray crystal structures of SPU inhibited by all the catechol derivatives analysed in this work, as well as by catechol itself [17i], with the crystal structure of native SPU (4CEU, [16]), shows that all catechol derivatives replace four water molecules located in the corridor formed by the thiol of αCys322 and the side chain of αLys169, a volume used by the mobile flap to close towards the di-nickel active site during the hydrolytic event of urease catalysis. Interestingly, W_A and W_B are also present and not perturbed in the native structure.

In the structures containing compounds **3MC**, **4MC**, **3,4DMC**, **3,5DMC and 4,5DMC**, the S-C bond is formed between the thiol group of αCys322 and the C atom in *ortho* to one of the catechol derivatives hydroxyl groups, an observation that supports the originally proposed reaction mechanism [17i] (Scheme 4):
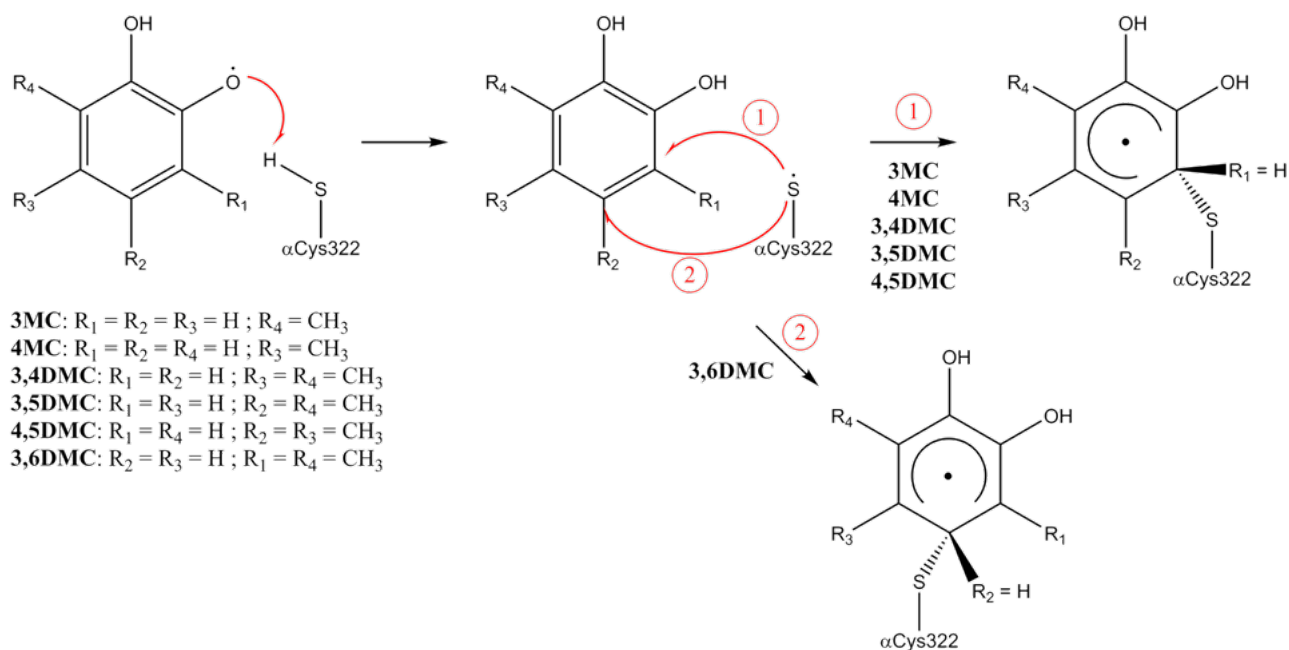
Scheme 4: Proposed mechanism for the radical reaction between a semiquinone derivative and the thiol group of αCys322 in SPU.

In the first step, the thiol hydrogen of αCys322 is removed by the radical oxylic group of the semiquinone derivative, previously formed by oxidation of the starting catechol derivative by molecular oxygen, to give the reduced form of the latter and a sulfanyl radical (αCys322-S•). In the second step, the S atom of αCys322-S• then attacks the *ortho* carbon atom of the catechol derivative (reaction path 1: carbon number 3 in the case of **4MC** and **4,5DMC** and carbon 6 in the case of **3MC**, **3,4DMC** and **3,5DMC**), a step facilitated by the formation of an H-bond between the S atom and the aromatic OH group, to give a reaction intermediate radical. The latter could eventually react with either molecular oxygen (to give a hydroperoxyl radical) or another molecule of semiquinone derivative (to give the fully reduced catechol-derivative moiety), or the fully oxidized form of the catechol derivative (to give the semiquinone derivative), all cases involving the extraction of a radical H atom to give the reaction products observed in the crystal structures described above. The only exception to this rule is represented by **3,6DMC** (reaction path 2) for which the aromatic C atom forming the thioether moiety with αCys322 is in the *meta* position (carbon number 4) with respect to

13

the hydroxyl groups. In this case, the H atoms in the *ortho* positions are substituted by methyl groups, much worse leaving groups than H atoms. Moreover, the formation of the H-bond between the S atom in the sulfanyl radical and the hydroxyl group on catechol, assisting the attack on the *ortho* position, is impeded by steric hindrance due to the presence of the methyl groups.

The kinetic data shown in Figure 2 indicate that the most efficient inhibitor is **3MC**, followed, in order of decreasing efficiency, by **4,5DMC**, **4MC**, **3,4DMC**, **CAT**, **3,5DMC** and finally **3,6DMC.** The previously reported data analysis for the urease inactivation by catechol, performed using Eq. 1 and a simultaneous global fit of all the data at different inhibitor concentrations, yielded values for k_1 and k_2; these represent functions of the single kinetic constants that regulate each step of the inactivation mechanism (Scheme 1) [17i]. In the case of the mono- and di-substituted catechols studied in this work, the same global fit did not return satisfactory results. However, by analysing the data collected at 20 μM inhibitors concentration, we observed that the obtained values of the $k_1 \cdot k_2$ product (Table 5-SI) consistently correlates with the inactivation proficiency of the catechol derivatives **3MC > 4,5DMC > 3,4DMC > 4MC > CAT > 3,5DMC > 3,6DMC**, indicating that this parameter can be empirically used to compare the efficacy of the compounds tested.

In an attempt to rationalize these results on the basis of the electron spin distribution in the corresponding semiquinones, and therefore of the reactivity of this radical intermediate with thiols, quantum mechanical calculations were carried out. All stable conformations of the semiquinone form were considered for the six inhibitors studied in this work. The results of these calculations indicate that the largest portion of spin density is localized on the radical oxylic group for all the semiquinone derivatives and in all the considered conformations (see Tables 6-SI – 17-SI and Figure 6-SI). This observation supports the reaction mechanism illustrated in Scheme 1.

In order to get a deeper insight into the effects of the methyl substituents on the catechol aromatic ring, the structures of all the possible reaction intermediates (*i.e.* the chemical species achieved at the end of the reaction path depicted in Scheme 4, before the final step of the reaction) were calculated for each of the substituted catechols considered in this work (see Figure 7-SI and 8-SI). In all cases,

the formation energy of the reaction intermediate leading to the final compound observed in the corresponding crystal structure is lower than the other possible reaction intermediates (see Table 18-SI). Moreover, the formation energies of the most stable intermediate of the mono- and the di-substituted catechols are in good agreement with the kinetic data. In particular, the formation energy of the **3MC** intermediate is lower than that of **4MC** intermediate. For the intermediates derived from the di-substituted catechols, the formation energies follow the order **3,4DMC < 4,5DMC < 3,5DMC < 3,6DMC** (Table 18-SI). However, the formation energy of the intermediate does not provide information on the activation energy of the reaction, and the mono-substituted catechol intermediates are not comparable with the non-substituted or with the di-substituted catechols. For this reason, starting from the optimized structure of the reaction intermediates, the energy profile of the dissociation of the carbon-sulphur bond of each intermediate was studied by performing relaxed surface scan computations [25]. These were done by slowly increasing the bond distance of the bound C and S atoms from 1.5 to 4.5 Å and optimizing all the remaining coordinates. Considering the high computational cost of such calculations, the basis set was changed from the one used for the single point computations (aug-cc-pVTZ) to a less expensive set [6-311G(d,p)]. The results of the relaxed scans are shown in Figure 5 and in Table 19-SI. The trend of the energy barriers required to move from the (substituted) catechol reacting with the $CH_3S\bullet$ moiety to the relative energy maxima is in good agreement with the kinetic data. Moreover, in this way it is possible to compare the catechol data [17i] with the energy barriers of all the substituted catechols considered in the present study. The DFT modelling results described above rely on gas-phase calculations in which neither explicit nor implicit interactions of the catechol molecules with the solvent or with the active site residues are included; moreover, the minimal CH_3SH cysteine model, together with the relaxed scan optimization, does not account for energetic effects of the protein-bound catechol *vs*. cysteine positioning. Therefore, the calculated relative energy differences thus obtained must be taken *cum grano salis*, because the energy order of the configurations could be affected by protein-specific effects not considered in the DFT model scheme used. These considerations notwithstanding, the relative

intermediate stabilities thus obtained are found to be consistent with the observed overall inhibition kinetic data.

CONCLUSIONS

In this paper, a structural characterization of the inactivation of the bacterial urease from *Sporosarcina pasteurii* by mono- and di-substituted catechol derivatives has been carried out. The structural information was supported by both kinetic studies, performed on a plant urease (*Canavalia ensiformis*, JBU) and by computational quantum mechanical calculations. This integrated approach indicates that catechol derivatives inactivate urease by blocking the mobile flap in an open position, thus impeding the modulation of the passage of substrate/products to and from the active site, through the formation of a covalent adduct on the conserved αCys322 residue through a radical-based mechanism. These results, obtained in this work for mono- and di-substituted catechol derivatives, suggest a common behaviour of several aromatic poly-hydroxylated urease inhibitors and indicate that a single electron donating substituent on the catechol aromatic ring in the 3-position is the best solution to significantly improving the inhibition capability of this class of inhibitors.

The high conservation of the mobile flap cysteine residues in ureases from numerous organisms, such as *Helicobacter pylori* and other pathogenic bacteria listed by WHO as antibiotic-resistance threats, render these results of wide interest. This information is essential for the development of novel urease inhibitors based on the catechol scaffold by structure-based design and structure–activity relationship studies, with potential fallouts both for medicine and for agro-environmental purposes.

Figure 1. Conformation of the mobile flap of SPU in the open (A) and in the closed (B) state (PDB codes 4CEU and 3UPB, respectively). Left panels: SPU molecular surface coloured in coral, turquoise and light green for subunit α, β and γ, respectively. The mobile flap surface in subunit α is in dark red. Right panels: ribbon diagram and longitudinal section of the molecular surface in the binding site region. The side chains of αLys220*, αCys322 and αHis323 are in sticks coloured according to atom type. The Ni(II) ions are shown as green spheres.
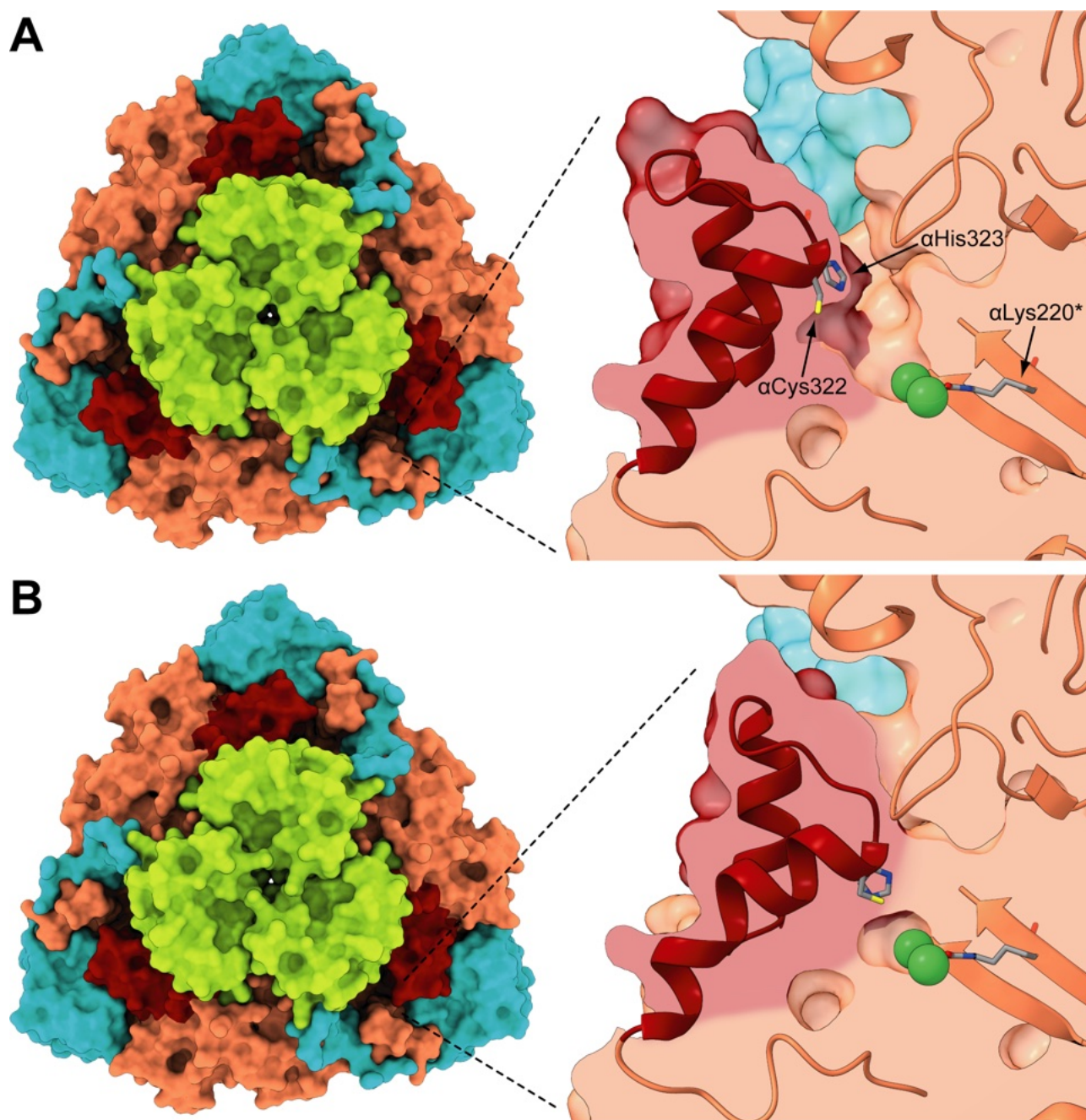
Figure 2. Plots of JBU residual activity *vs.* incubation time with a fixed 20 µM concentration of (in order of increasing inhibition capabilities) **3,6DMC** (purple circles), **3,5DMC** (red circles), **4MC** (green circles), **3,4DMC** (cyan circles), **4,5DMC** (light blue circles), and **3MC** (dark blue circles). The same data already published for **CAT** [17i] (orange circles) at the same concentration are reported as a comparison. The lines represent the result of the data fits using Eq. (1).
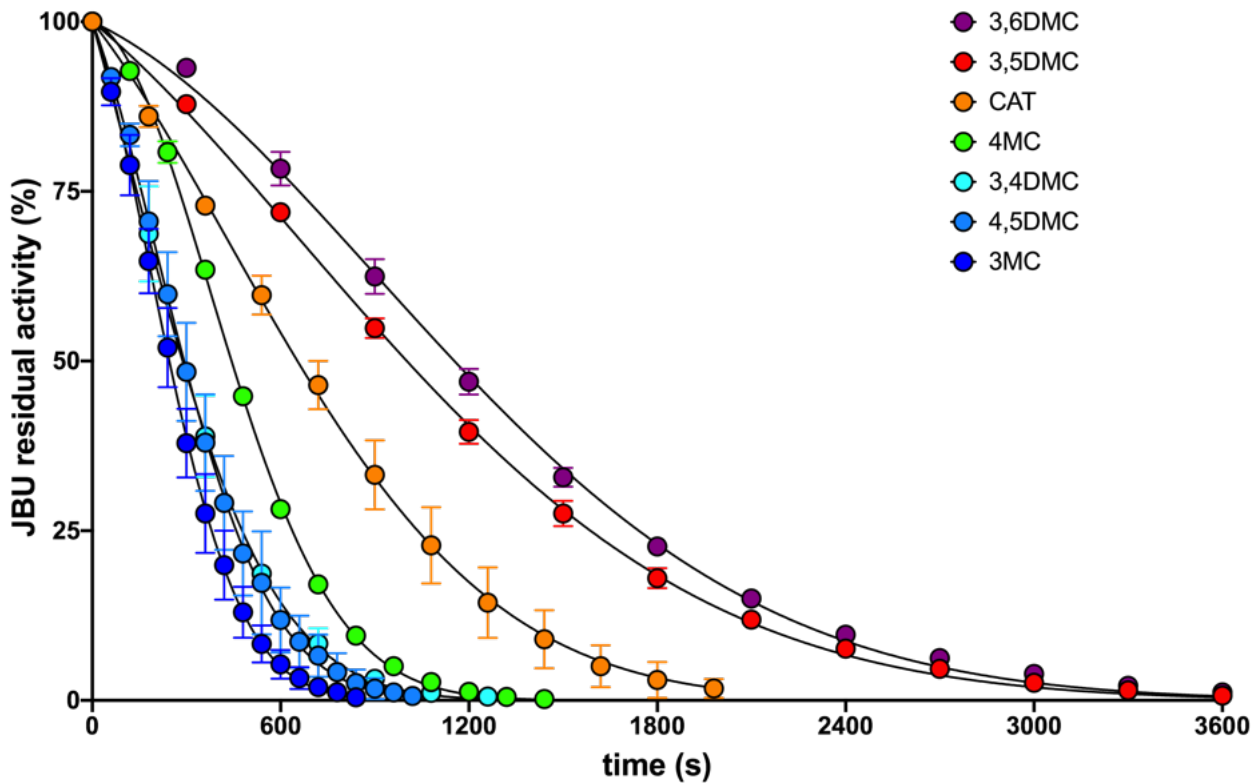
Figure 3. Atomic models of the active site of SPU bound to **3MC** (A), **4MC** (B), **3,4DMC** (C), **3,5DMC** (D), **4,5DMC** (E), and **3,6DMC** (F) (PDB codes 6ZNY, 6ZNZ, 6ZO0, 6ZO1, 6ZO2 and 6ZO3). The carbon, nitrogen, oxygen, sulphur and nickel atoms are grey, blue, red, yellow and green, respectively. The nickel-coordination environment is shown superimposed on the final $2F_o - F_c$ electron density map contoured at 1σ; the map for the inhibitor is shown coloured in yellow.
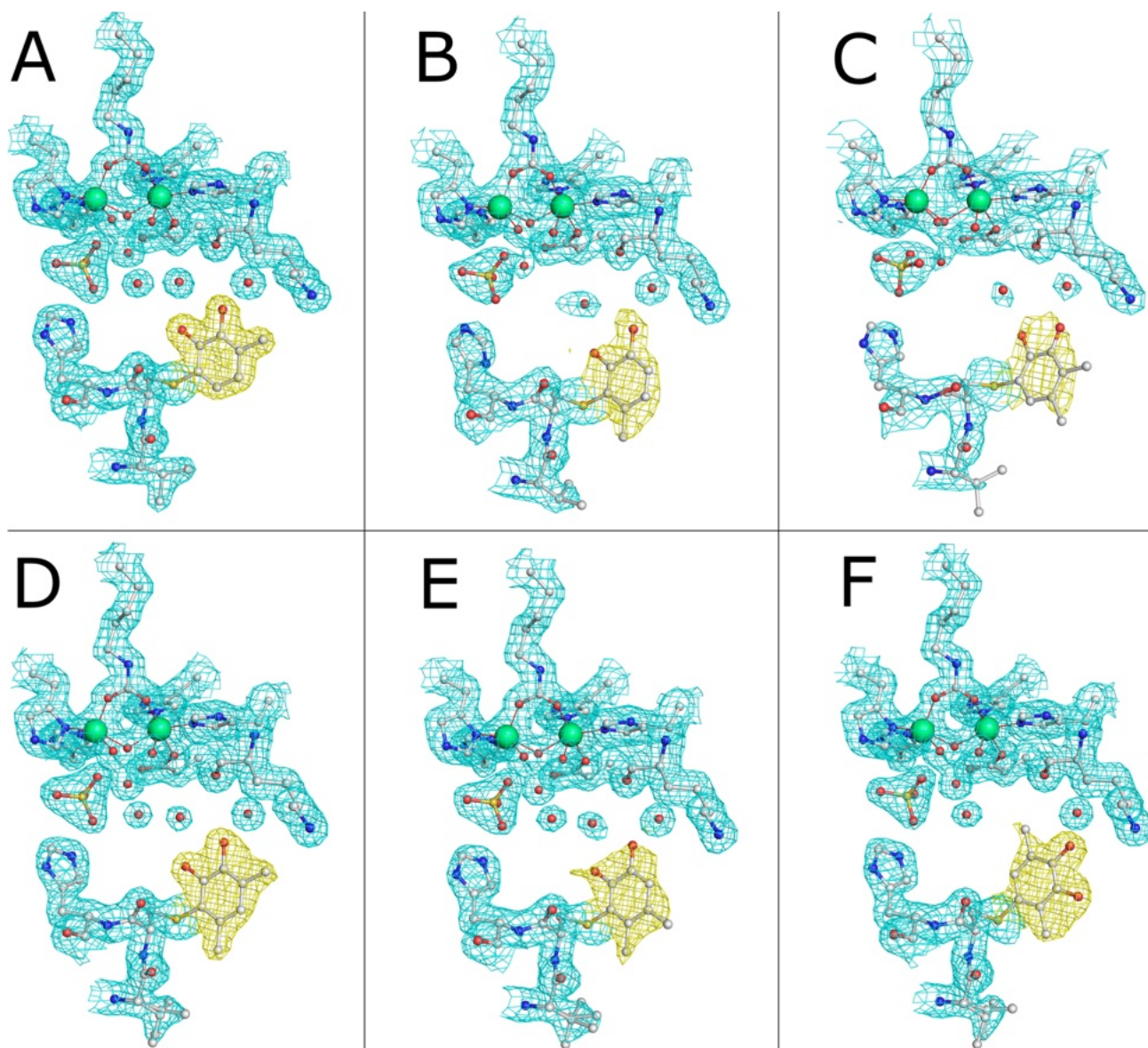
Figure 4. Crystallographic structures of the active site of SPU bound to **3MC** (A), **4MC** (B), **3,4DMC** (C), **3,5DMC** (D), **4,5DMC** (E), and **3,6DMC** (F) (PDB codes 6ZNY, 6ZNZ, 6ZO0, 6ZO1, 6ZO2 and 6ZO3). Putative hydrogen bonds are shown as thin blue lines. Spheres are drawn using the relative-atomic-radius values in CrystalMaker. The carbon, nitrogen, oxygen, sulphur, and nickel atoms are coloured grey, blue, red, yellow, and green, respectively.
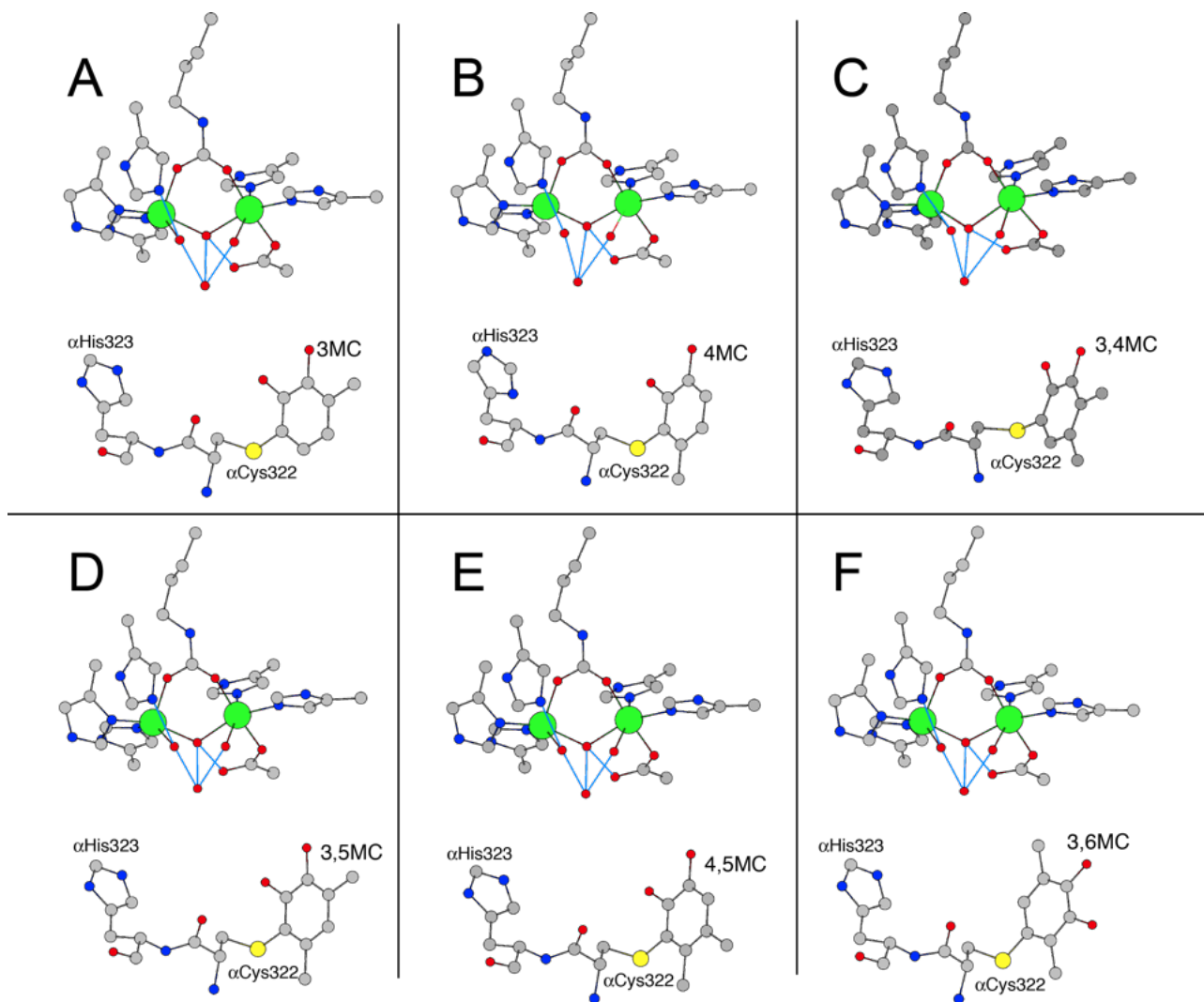
Figure 5. Results of the relaxed surface scan computations along the reaction pathways between the mono- and di-substituted catechols studies in this work and the methyl-sulfanyl radical.
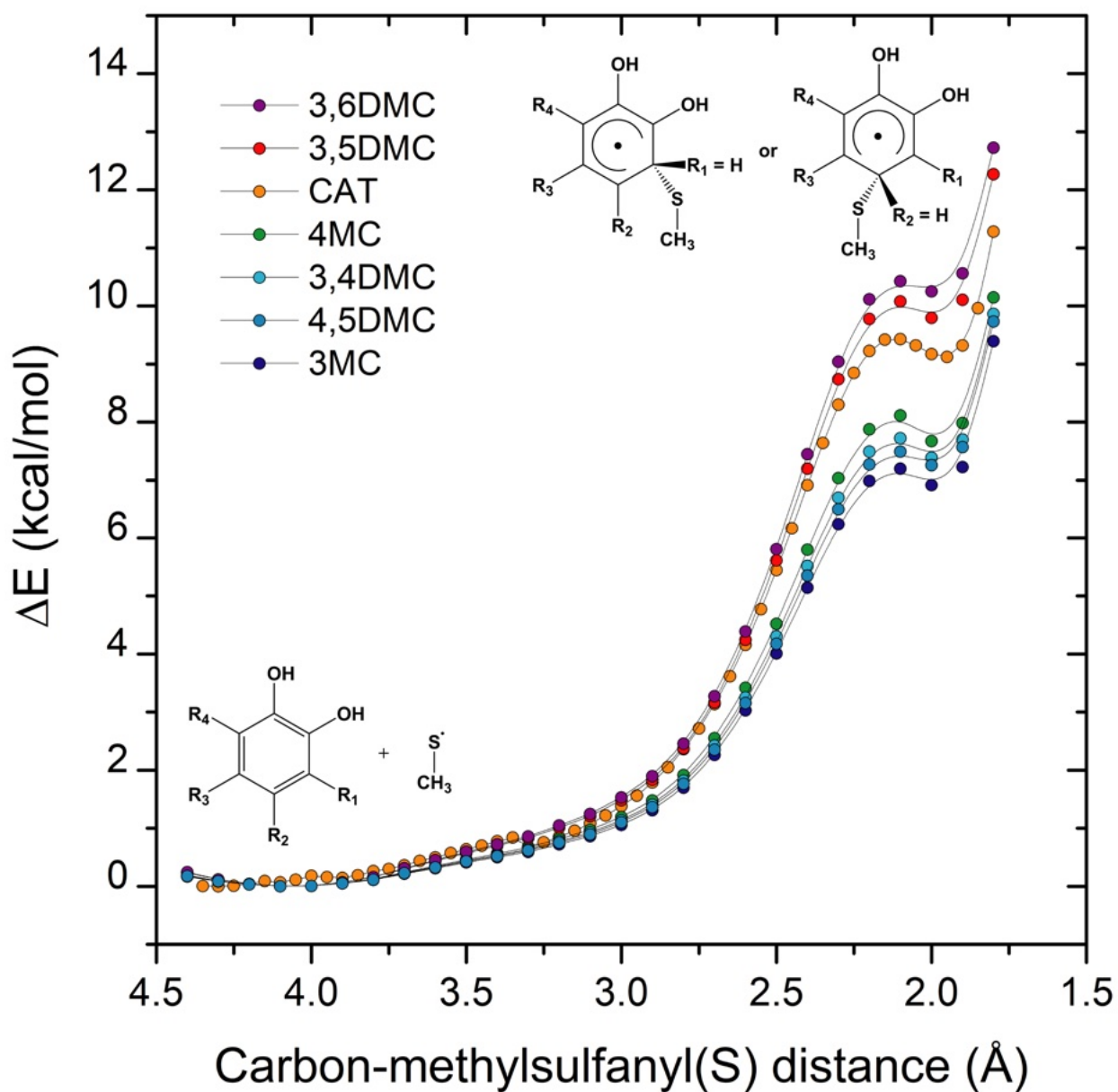
REFERENCES

[1]   a R. P. Hausinger, *Microbiol. Rev.* **1987**, *51*, 22-42; b H. L. Mobley, R. P. Hausinger, *Microbiol. Rev.* **1989**, *53*, 85-108.

[2]   a R. L. Blakeley, J. A. Hinds, H. E. Kunze, E. C. Webb, B. Zerner, *Biochemistry* **1969**, *8*, 1991-2000; b N. E. Dixon, P. W. Riddles, C. Gazzola, R. L. Blakeley, B. Zerner, *Can. J. Biochem.* **1980**, *58*, 1335-1344; c M. J. Maroney, S. Ciurli, *Chem. Rev.* **2014**, *114*, 4206-4228; d L. Mazzei, F. Musiani, S. Ciurli, in *The Biological Chemistry of Nickel* (Eds.: D. Zamble, M. Rowińska-Żyrek, H. Kozłowski), Royal Society of Chemistry, **2017**, pp. 60-97; e L. Mazzei, F. Musiani, S. Ciurli, *J Biol Inorg Chem* **2020**, *25*, 829-845.

[3]   J. C. Rutherford, *PLoS Pathog.* **2014**, *10*, e1004062.

[4]   S. Kiss, M. Simihaian, *Improving efficiency of urea fertilizers by inhibition of soil urease activity*, Kluwer Academic Publishers, Dordrecht, The Netherlands, **2002**.

[5]   a I. Konieczna, P. Zarnowiec, M. Kwinkowski, B. Kolesinska, J. Fraczyk, Z. Kaminski, W. Kaca, *Curr. Protein Pept. Sci.* **2012**, *13*, 789-806; b R. J. Maier, S. L. Benoit, *Inorganics* **2019**, *7*, 80.

[6]   a P. Bauerfeind, R. Garner, B. E. Dunn, H. L. T. Mobley, *Gut* **1997**, *40*, 25-30; b B. Marshall, J. R. Warren, *The Lancet* **1984**, *323*, 1311-1315; c K. Stingl, K. Altendorf, E. Bakker, *Trends Microbiol.* **2002**, *10*, 70-74.

[7]   C. Zhou, F. Bhinderwala, M. K. Lehman, V. C. Thomas, S. S. Chaudhari, K. J. Yamada, K. W. Foster, R. Powers, T. Kielian, P. D. Fey, *PLoS Pathog* **2019**, *15*, e1007538.

[8]   a A. H. Gordon, P. D. Hart, M. R. Young, *Nature* **1980**, *286*, 79-80; b D. L. Clemens, B. Y. Lee, M. A. Horwitz, *J. Bacteriol.* **1995**, *177*, 5644-5652; c W. Lin, V. Mathys, E. L. Y. Ang, V. H. Q. Koh, J. M. Martínez Gómez, M. L. T. Ang, S. Z. Zainul Rahim, M. P. Tan, K. Pethe, S. Alonso, *Infect. Immun.* **2012**, *80*, 2771-2779.

[9]   G. Young, D. Amid, V. Miller, *J. Bacteriol.* **1996**, *178*, 6487-6495.

[10] G. M. Cox, J. Mukherjee, G. T. Cole, A. Casadevall, J. R. Perfect, *Infect. Immun.* **2000**, *68*, 443-448.

[11] WHO, **2017**.

[12] F. Zhou, T. Yu, R. Du, G. Fan, Y. Liu, Z. Liu, J. Xiang, Y. Wang, B. Song, X. Gu, L. Guan, Y. Wei, H. Li, X. Wu, J. Xu, S. Tu, Y. Zhang, H. Chen, B. Cao, *The Lancet* **2020**, *395*, 1054-1062.

[13] F. Paulot, D. J. Jacob, *Environ. Sci. Technol.* **2014**, *48*, 903-908.

[14] Y. Cui, Z. F. Zhang, J. Froines, J. Zhao, H. Wang, S. Z. Yu, R. Detels, *Environ Health* **2003**, *2*, 15.

[15] L. Mazzei, M. Cianci, A. Gonzalez Vara, S. Ciurli, *Dalton Trans* **2018**, *47*, 8240-8247.

[16] S. Benini, M. Cianci, L. Mazzei, S. Ciurli, *J. Biol. Inorg. Chem.* **2014**, *19*, 1243-1261.

[17] a S. Benini, W. R. Rypniewski, K. S. Wilson, S. Ciurli, S. Mangani, *J. Biol. Inorg. Chem.* **1998**, *3*, 268-273; b S. Benini, W. R. Rypniewski, K. S. Wilson, S. Miletti, S. Ciurli, S. Mangani, *Structure* **1999**, *7*, 205-216; c S. Benini, W. R. Rypniewski, K. S. Wilson, S. Miletti, S. Ciurli, S. Mangani, *J. Biol. Inorg. Chem.* **2000**, *5*, 110-118; d S. Benini, W. R. Rypniewski, K. S. Wilson, S. Ciurli, S. Mangani, *J. Biol. Inorg. Chem.* **2001**, *6*, 778-790; e S. Benini, W. R. Rypniewski, K. S. Wilson, S. Mangani, S. Ciurli, *J. Am. Chem. Soc.* **2004**, *126*, 3714-3715; f L. Mazzei, M. Cianci, S. Benini, L. Bertini, F. Musiani, S. Ciurli, *J. Inorg. Biochem.* **2016**, *154*, 42-49; g L. Mazzei, M. Cianci, F. Musiani, S. Ciurli, *Dalton Trans.* **2016**, *45*, 5455-5459; h L. Mazzei, M. Cianci, U. Contaldo, F. Musiani, S. Ciurli, *Biochemistry* **2017**, *56*, 5391-5404; i L. Mazzei, M. Cianci, F. Musiani, G. Lente, M. Palombo, S. Ciurli, *J. Inorg. Biochem.* **2017**, *166*, 182-189; j L. Mazzei, M. N. Wenzel, M. Cianci, M. Palombo, A. Casini, S. Ciurli, *ACS Med. Chem. Lett.* **2019**, *10*, 564-570; k L. Mazzei, M. Cianci, U. Contaldo, S. Ciurli, *J Agric Food Chem* **2019**, *67*, 2127-2138; l L. Mazzei, M. Cianci, S. Benini, S. Ciurli, *Chemistry* **2019**, *25*, 15351-15360.

[18] L. Mazzei, M. Cianci, S. Benini, S. Ciurli, *Angew. Chem. Int. Ed.* **2019**, *58*, 7415-7419.

[19]   F. Musiani, E. Arnofi, R. Casadio, S. Ciurli, *J. Biol. Inorg. Chem.* **2001**, *6*, 300-314.

[20]   S. Benini, P. Kosikowska, M. Cianci, L. Mazzei, A. G. Vara, L. Berlicki, S. Ciurli, *J Biol Inorg Chem* **2013**, *18*, 391-399.

[21]   R. Puupponen-Pimiä, A. M. Aura, K. M. Oksman-Caldentey, P. Myllärinen, M. Saarela, T. Mattila-Sandholm, K. Poutanen, *Trends in Food Science & Technology* **2002**, *13*, 3-11.

[22]   a E. Pastene, H. Speisky, A. García, J. Moreno, M. Troncoso, G. Figueroa, *Journal of Agricultural and Food Chemistry* **2010**, *58*, 7172-7179; b L. Paulo, M. Oleastro, E. Gallardo, J. Queiroz, F. Domingues, *Food Res. Int.* **2011**, *44*, 964–969; c M. Daglia, *Curr. Opin. Biotechnol.* **2012**, *23*, 174-181; d F. Cardona, C. Andrés-Lacueva, S. Tulipani, F. Tinahones, M. Queipo-Ortuño, *J. Nutr. Biochem.* **2013**, *24*, 1415-1422.

[23]   I. Masafumi, U. Daisuke, I. Masayuki, *Heterocycles* **2010**, *82*, 491-504.

[24]   A. Pezzella, L. Lista, A. Napolitano, M. d'Ischia, *Tetrahedron Lett.* **2005**, *46*, 3541-3544.

[25]   F. Neese, *Wiley Interdiscip. Rev.: Comput. Mol. Sci.* **2012**, *2*, 73-78.

[26]   a A. D. Becke, *J. Chem. Phys.* **1993**, *98*, 1372-1377; b C. Lee, W. Yang, R. G. Parr, *Phys. Rev. B* **1988**, *37*, 785-789.

[27]   M. J. Frisch, G. W. Trucks, H. B. Schlegel, G. E. Scuseria, M. A. Robb, J. R. Cheeseman, G. Scalmani, V. Barone, G. A. Petersson, H. Nakatsuji, X. Li, M. Caricato, A. V. Marenich, J. Bloino, B. G. Janesko, R. Gomperts, B. Mennucci, H. P. Hratchian, J. V. Ortiz, A. F. Izmaylov, J. L. Sonnenberg, Williams, F. Ding, F. Lipparini, F. Egidi, J. Goings, B. Peng, A. Petrone, T. Henderson, D. Ranasinghe, V. G. Zakrzewski, J. Gao, N. Rega, G. Zheng, W. Liang, M. Hada, M. Ehara, K. Toyota, R. Fukuda, J. Hasegawa, M. Ishida, T. Nakajima, Y. Honda, O. Kitao, H. Nakai, T. Vreven, K. Throssell, J. A. Montgomery Jr., J. E. Peralta, F. Ogliaro, M. J. Bearpark, J. J. Heyd, E. N. Brothers, K. N. Kudin, V. N. Staroverov, T. A. Keith, R. Kobayashi, J. Normand, K. Raghavachari, A. P. Rendell, J. C. Burant, S. S. Iyengar, J. Tomasi, M. Cossi, J. M. Millam, M. Klene, C. Adamo, R. Cammi, J. W.

Ochterski, R. L. Martin, K. Morokuma, O. Farkas, J. B. Foresman, D. J. Fox, Wallingford, CT, **2016**.